

## Design and optimization of weakly coupled multi-core fiber

ZHAN Yi, WANG An, ZHANG Qing-long, WANG Yi-han

Citation:

ZHAN Yi, WANG An, ZHANG Qing-long, WANG Yi-han. Design and optimization of weakly coupled multi-core fiber[J]. *Chinese Optics*, In press. doi: 10.37188/CO.EN-2026-0006

詹仪, 王安, 张清龙, 王奕涵. 弱耦合多芯光纤的设计与优化[J]. *中国光学*, 优先发表. doi: 10.37188/CO.EN-2026-0006

View online: <https://doi.org/10.37188/CO.EN-2026-0006>

---

## Articles you may be interested in

[Advances in optical fiber tweezer technology based on hetero-core fiber](#)

特种芯光纤光镊技术研究进展

*Chinese Optics*. 2023, 16(6): 1293 <https://doi.org/10.37188/CO.2023-0016>

[Capillary liquid-core optical fiber temperature sensor based on fluorescence intensity ratio](#)

基于荧光强度比的毛细管液芯光纤温度传感器

*Chinese Optics*. 2024, 17(3): 528 <https://doi.org/10.37188/CO.2023-0160>

[Review of crosstalk between pixels in division of focal plane polarization camera](#)

分焦平面偏振相机的像素间串扰研究进展

*Chinese Optics*. 2025, 18(4): 725 <https://doi.org/10.37188/CO.2024-0217>

[Design optimization of a sensitivity-enhanced tilt sensor based on femtosecond fiber bragg grating](#)

基于飞秒光纤光栅的增敏型倾角传感器设计与优化

*Chinese Optics*. 2025, 18(4): 908 <https://doi.org/10.37188/CO.EN-2024-0034>

[Multi-channel optical switching based on scanning mirror instrumentation](#)

基于扫描反射镜结构的多路光开关

*Chinese Optics*. 2023, 16(1): 136 <https://doi.org/10.37188/CO.2022-0020>

[Design and optimization of Micro LED vehicle light projection optical system](#)

Micro LED车灯投影光学系统设计与优化

*Chinese Optics*. 2024, 17(1): 89 <https://doi.org/10.37188/CO.2023-0063>

文章编号 2097-1842(xxxx)x-0001-15

## Design and optimization of weakly coupled multi-core fiber

ZHAN Yi\*, WANG An, ZHANG Qing-long, WANG Yi-han

(College of Engineering, Qufu Normal University, Rizhao 276800, Shandong, China)

\* Corresponding author, E-mail: zhanyi@qfnu.edu.cn

**Abstract:** In order to achieve comprehensive, highly efficient, and multi-objective precise optimization of fiber structural parameters and further enhance the transmission capacity of optical communication systems, a homogeneous weakly coupled seven-core fiber based on trench-assisted structures is designed. Particle Swarm Optimization (PSO) is introduced to replace traditional empirical designs or local scanning methods. First, a multi-objective fitness function incorporating constraints such as dispersion, cutoff wavelength, effective mode field area, and coating loss is established. Then, the algorithm performs a global search to precisely determine the optimal structural parameters under standard dimensional constraints. Simulation results demonstrate that with a fiber core pitch of 45  $\mu\text{m}$ , the optimized fiber achieves an ultra-low inter-core crosstalk of below  $-90$  dB/km at a wavelength of 1550 nm. This design scheme not only effectively resolves the conflict between crosstalk suppression and spatial utilization in multi-core fibers but also proves the efficiency and reliability of the PSO algorithm in complex fiber structural design, providing an important theoretical basis and technical support for the research and manufacturing of ultra-large-capacity optical communication systems.

**Key words:** multi-core fiber; particle swarm optimization; trench-assisted; inter-core crosstalk; space division multiplexing

## 弱耦合多芯光纤的设计与优化

詹 仪\*, 王 安, 张清龙, 王奕涵

(曲阜师范大学工学院, 山东日照 276800)

**摘要:**为实现光纤结构参数的全面、高效及多目标精确优化,并进一步提升光通信系统的传输容量,本文引入粒子群优化算法(PSO)代替传统经验设计或局部扫描方法,设计一种基于沟槽辅助结构的同质弱耦合七芯光纤。在建立一个包含色散、截止波长、有效模场面积和涂层损耗等约束条件的多目标适应度函数的基础上,利用粒子群优化算法进行全局搜索,在标准尺寸约束下精确确定光纤的最佳结构参数。仿真结果表明:在光纤纤芯间距为 45  $\mu\text{m}$  时,优化后的光纤在 1550 nm 波长处实现了低于  $-90$  dB/km 的超低芯间串扰,有效解决了多芯光纤中串扰抑制与空间利用率之间的冲突,证明了粒子群算法在复杂光纤结构设计中的高效性与可靠性,为超大容量光纤通信系统的研发与制造提供了重要的理论依据和技术支持。

收稿日期:2026-01-12; 修订日期:xxxx-xx-xx

基金项目:山东省自然科学基金(No. ZR2020MF107)

Supported by Natural Science Foundation of Shandong Province (No. ZR2020MF107)

关键词: 多芯光纤; 粒子群优化; 沟槽辅助; 芯间串扰; 空分复用

中图分类号: TN253

文献标志码: A

doi: 10.37188/CO.EN-2026-0006

CSTR: 32171.14.CO.EN-2026-0006

## 1 Introduction

With the rapid development of communication networks, optical fiber, as a vital transmission medium for optical signals, plays a crucial role in optical communications. The transmission capacity of traditional single-mode fibers is approaching its limit and is no longer sufficient to meet current demands for communication capacity. To enhance the transmission capacity of optical fibers and achieve better transmission performance, multi-core technology based on the principle of Space Division Multiplexing (SDM) has emerged<sup>[1-2]</sup>. SDM is considered a promising technology capable of significantly increasing network capacity and overcoming the capacity limitations faced by traditional optical fiber communication networks.

MCF is designed as one of the transmission media for the system, aiming to address the capacity limits of traditional single-mode fibers by increasing the number of cores and fully utilizing the spatial dimension, thereby multiplying the transmission capacity of the fiber<sup>[3-5]</sup>. However, due to the limited thickness of the cladding, as the number of cores increases, the distance between cores becomes smaller. The design around each core allows optical signals to effectively couple and exchange between adjacent cores, which cannot support long-distance multi-mode transmission. Therefore, compared to strongly coupled MCF, weakly coupled MCF—by virtue of having larger core-to-core pitch can effectively reduce crosstalk between signals. This contributes to enhancing system stability, especially in long-distance transmission. Each core can be viewed as an independent channel with minimal interference, eliminating the need for complex Multiple-Input Multiple-Output (MIMO) signal processing. In addition to increasing the core pitch, sup-

pressing inter-core crosstalk is also an unavoidable issue in MCF design. The main methods include trench-assisted<sup>[6-7]</sup>, air-hole assisted<sup>[8]</sup>, and heterogeneous structure fibers<sup>[9]</sup>. Both trench-assisted and air-hole assisted methods confine energy within the fiber core by increasing the refractive index difference between the core and its surrounding environment.

In 2010, Hokkaido University and Nippon Telegraph and Telephone Corporation (NTT) proposed a theoretical model for weakly coupled MCFs based on air-hole assistance, proving that a dual-core fiber with air-hole assistance could achieve a coupling length of tens of kilometers in the 1550 nm band, effectively suppressing inter-core crosstalk<sup>[10]</sup>. In 2011, K. Takenaga et al. from Fujikura simulated and manufactured a trench-assisted seven-core fiber<sup>[11]</sup>, confirming the immense potential of trench-assisted MCF in achieving large-capacity, long-distance optical transmission. In 2012, Hokkaido University designed a weakly coupled 12-core single-mode fiber by adding trench-assisted structures to heterogeneous cores<sup>[12]</sup>. With a core pitch of 33  $\mu\text{m}$ , the inter-core crosstalk at 1550 nm was as low as  $-42$  dB/km, exhibiting excellent bending resistance and anti-nonlinearity performance. In 2019, Sumitomo Electric and the US silicon photonics semiconductor company Luxtera demonstrated a transmission scheme based on a rectangular weakly coupled eight-core fiber at the European Conference on Optical Communication (ECOC)<sup>[13]</sup>. The cores utilized a channel-assisted refractive index design to suppress inter-core crosstalk, with a core pitch ranging from 35 to 45  $\mu\text{m}$ , achieving inter-core crosstalk below  $-66$  dB/km at 1310 nm. In 2016, Feihong Ye et al. proposed a theoretical analysis model for homogeneous trench-assisted MCF based on coupled-mode theory<sup>[14]</sup>. This model can analyze the relationship between inter-core crosstalk and

parameters such as trench depth, trench width, and core structure, providing a powerful theoretical tool for designing high-core-count homogeneous trench-assisted MCFs. However, despite the progress made in these studies, significant limitations still exist in the design process. Most existing methods, including the aforementioned works, either rely on complex heterogeneous core structures that are difficult to manufacture or employ optimization methods that involve only a subset of parameters describing the refractive index distribution. Due to the lack of a global optimization strategy that considers all structural parameters simultaneously, the room for performance improvement is limited, and obtaining an optimal design while balancing ultra-low crosstalk with other transmission constraints remains a challenge.

Currently, standard cladding diameter (125  $\mu\text{m}$ ) weakly coupled MCFs range from 4 cores<sup>[15-16]</sup> to 8 cores<sup>[17-20]</sup>. This paper selects a homogeneous, standard-diameter, weakly coupled seven-core fiber as the optimization target, benefiting from its ultra-low inter-core crosstalk (XT) while also being compatible with existing standard single-mode fibers (SSMF) and SMF-based devices<sup>[15-17]</sup>. Each core essentially acts as a single-mode fiber, independently carrying optical signals for one channel, with complete single-mode transmission characteristics ( $LP_{01}$  mode). Numerical simulations performed using the Finite Element Method (FEM) show that each core of the MCF is surrounded by an identical low-refractive-index trench, with a cladding layer between the core and the trench. To efficiently search the entire parameter space and provide a systematic solution for the design of weakly coupled MCFs, this paper introduces the Particle Swarm Optimization (PSO) algorithm<sup>[21-22]</sup> to effectively reduce the number of evaluation permutations and optimize all design parameters. Our method allows for comprehensive exploration and optimization of the parameter space, significantly reducing the number of required evaluations.

## 2 Fiber Design

### 2.1 Fiber Structure

Although Space Division Multiplexing (SDM) technology seeks to increase the number of spatial channels, it has also given rise to another major research direction: Randomly Coupled Multi-Core Fiber. Randomly coupled MCF is defined as an optical fiber where the optical pulse width evolves with the square root of the transmission distance, caused by random inter-core coupling induced by bending and twisting<sup>[23-24]</sup>. To strictly define the coupling state from a physical mechanism, the coupling length  $L_C$  is introduced as a benchmark, where  $L_C = \pi/2k$  and  $k$  is the mode coupling coefficient. In strongly coupled or randomly coupled fibers, the coupling length is typically short; whereas weakly coupled fibers are characterized by a coupling length ranging from  $10^2$  to  $10^3$  m.

In this context, we further define weakly coupled MCFs as fibers where inter-core coupling is significantly weaker than that of randomly coupled MCFs. Unlike randomly coupled MCFs that require complex MIMO (Multiple-Input Multiple-Output) signal processing, the weakly coupled design significantly reduces inter-core crosstalk, thereby eliminating the need for complex MIMO and reducing system complexity. By introducing a trench-assisted structure to suppress crosstalk, this design ensures high performance and compatibility with standard single-mode systems.

Fig. 1 illustrates the schematic of the optimized trench-assisted seven-core fiber. In this fiber structure  $n_{co}$ , and  $n_{cl}$  represent the refractive indices of the core and cladding, respectively, while  $k_1$ ,  $k_2$  and  $k_3$  denote the coupling coefficients between adjacent, spaced, and distant cores, respectively. By utilizing the refractive index profile ( $n_{co}, n_{cl}, n_{tr}$ ) and coupling coefficients ( $k_1, k_2, k_3$ ), the proposed model quantifies signal interference between cores at different locations. Fig. 2 displays the refractive in-

dex distribution of two adjacent cores with the trench-assisted structure. An inner cladding and a trench structure are introduced between the core and the outer cladding, where the refractive indices of the inner and outer claddings are equal. It is assumed that the core is Ge-doped and the trench is F-doped<sup>[25]</sup>, while both the inner and outer claddings are considered pure silica. Let the core radius be  $a_1$ , the inner cladding radius be  $a_2$  and the trench radius be  $a_3$ . This implies an inner cladding width of  $w_{cl} = a_2 - a_1$  and a trench width of  $w_{tr} = a_3 - a_2$ . The core refractive index is  $n_{co}$ , the cladding refractive index is  $n_{cl}$ , the trench refractive index is  $n_{tr}$ , the core pitch is  $\Lambda$ , the relative refractive index difference between the cladding and the core is  $\Delta_1$ , and the relative refractive index difference between the cladding and the trench is  $\Delta_2$ . The formulas for calculating  $\Delta_1$  and  $\Delta_2$  are shown in Eq (1) and (2):

$$\Delta_1 = \frac{n_{co}^2 - n_{cl}^2}{2n_{cl}^2}, \quad (1)$$

$$\Delta_2 = \frac{n_{tr}^2 - n_{cl}^2}{2n_{cl}^2}, \quad (2)$$

The cladding diameter is 125  $\mu\text{m}$ , and the Outer Cladding Thickness (OCT) is 30  $\mu\text{m}$ , to reduce coating loss and keep the additional loss caused by the coating below 0.001 dB/km<sup>[26]</sup>.

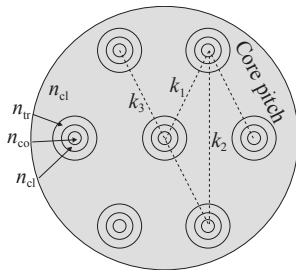


Fig. 1 Schematic of the optimized trench-assisted fiber

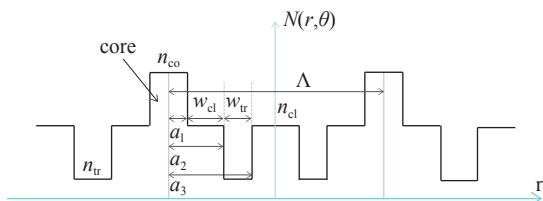


Fig. 2 Refractive index distribution

## 2.2 Parameter Selection

The flowchart of the PSO algorithm is shown in Fig. 3 (the fitness function and constraints will be detailed in Section 3). Each particle represents a potential solution, denoted as  $X_p$ . In this MCF design, each particle consists of a set of structural parameters for the MCF, containing six variables, with six parameters corresponding to each core type, as shown in Tab. 1. For each particle, the objective function is utilized to calculate its fitness value, which includes penalties for not meeting design constraints and the impact of crosstalk (XT). A smaller fitness value indicates better design quality for that particle. The optimization direction is described by velocity parameters. During the optimization process, each particle adjusts its optimization direction and position at each iteration according to Eq (3)<sup>[27]</sup>. The learning process of a particle is influenced by two factors: one is the best parameter set found by the particle so far ( $pbest$ ), and the other is the global best parameter set determined through global communication ( $gbest$ ). As the particles continuously learn to reduce their fitness values, when the particle swarm converges, the final optimal parameter set with the minimum fitness value can be found.

$$\begin{aligned} X'_p &= X_p + V'_p = \\ &X_p + [\omega V_p + c_1 \times rand_1 \times (pbest - X_p) + \\ &c_2 \times rand_2 \times (gbest - X_p)] \end{aligned}, \quad (3)$$

Here,  $rand_1$  and  $rand_2$  are uniform random numbers distributed on  $[0, 1]$ ;  $c_1$  and  $c_2$  are learning factors, both being constants;  $\omega$  is the inertia weight, used to balance the particle's global optimization ability and local optimization ability. According to reference<sup>[28]</sup>: the selection of these parameters is based on the constriction factor method proposed by Clerc and Kennedy. By setting the sum of learning factors  $\varphi = c_1 + c_2 > 4$ , the algorithm ensures particle convergence without requiring velocity clamping. In this study, we set  $c_1 = c_2 = 2.05$ , resulting in  $\varphi = 4.1$  and a constriction factor  $\omega = 0.729$ . This specific configuration mathematically balances the global

exploration ability and local exploitation ability of the particles. Furthermore, a sensitivity analysis regarding population size was conducted. Simulations indicated that a swarm size of 50 provides the optimal trade-off between calculation accuracy and

time consumption, as the fitness value stabilizes efficiently after approximately 60 iterations (as shown in Fig. 11).

$$\omega = \frac{2}{|2 - \varphi - \sqrt{\varphi(\varphi - 4)}|}, \quad (4)$$

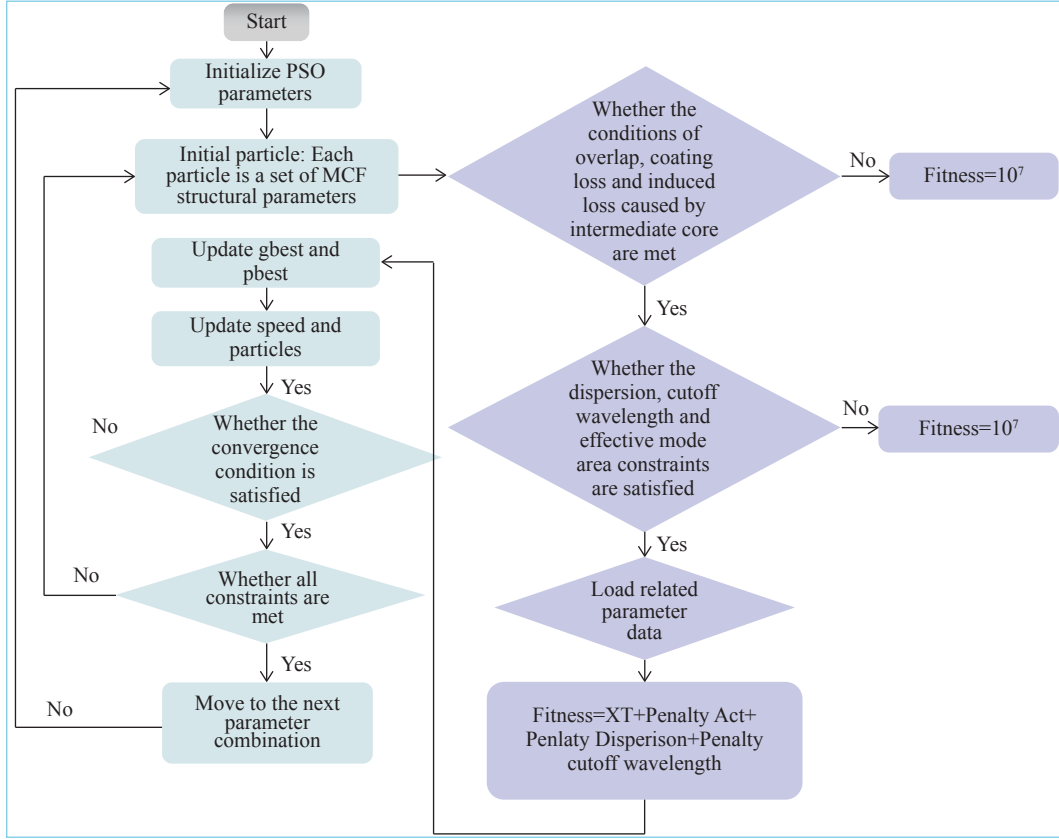


Fig. 3 Algorithm flow chart

Tab. 1 Parameter combination

Parameters	Range	Step	Choices
$a_1[\mu\text{m}]$	4~5	0.1	11
$w_{cl}[\mu\text{m}]$	2.5~7.5	0.1	51
$w_{tr}[\mu\text{m}]$	2.5~7.5	0.1	51
$\Delta_1$	0.3%~0.6%	0.01%	31
$\Delta_2$	-0.7%~-0.35%	0.01%	36
$\Lambda[\mu\text{m}]$	30~45	0.1	151

### 3 Combination of Objective Function and Constraints

#### 3.1 Calculation of Inter-core Crosstalk

The calculation of the mode coupling coeffi-

cient  $k_{pq}$  is the most critical and complex aspect of estimating inter-core crosstalk. Since the trench dimensions of the first cladding (inner cladding) and the trench-assisted structure are not infinite, the solutions for these two regions involve the modified Bessel function of the first kind<sup>[28]</sup>,  $I_0(W_1r/a_1)$ . The presence of modified Bessel functions makes the calculation of the mode coupling coefficient for trench-assisted MCF extremely difficult. If the effects of the first cladding and trench are neglected in  $I_0(W_1r/a_1)$ , the mode coupling coefficient between two adjacent cores in a homogeneous trench-assisted structure can be written as Eq (5)<sup>[29]</sup>:

$$k_{pq} = \frac{k(n_{co}^2 - n_{cl}^2)W_1 U_1 L_q \sqrt{\frac{\pi a_1}{2\Lambda W_1}} \exp\left(-W_1 \frac{\Lambda}{a_1}\right)}{n_m a_{1-m}^2 V_{1-m}^2 J_1^2(U_{1-m})} \times \int_0^{a_1} J_0\left(\frac{U_1}{a_1} r\right) I_0\left[\left(\frac{W_1}{a_1} - \frac{P_2 - P_1 + Y_2 - Y_1}{\Lambda - r}\right) r\right] \exp\left[\left(P_2 - P_1 + Y_2 - Y_1\right) \frac{\Lambda}{\Lambda - r}\right] r dr, \quad (5)$$

$L_q, P_1, P_2, Y_1, Y_2$  and  $P_1 - P_2 + Y_1 - Y_2$  can be expressed as:

$$L_q = \frac{J_1(U_1) K_1(W_1 a_2/a_1) K_1(W_2 a_3/a_1)}{K_1(W_1) K_1(W_2 a_2/a_1) K_1(W_1 a_3/a_1)}$$

$$P_1 = W_1 \frac{\Lambda - a_3}{a_1}, P_2 = W_2 \frac{\Lambda - a_3}{a_1}$$

$$Y_1 = W_1 \frac{\Lambda - a_2}{a_1}, Y_2 = W_2 \frac{\Lambda - a_2}{a_1}$$

$$P_1 - P_2 + Y_1 - Y_2 = (W_2 - W_1) \frac{a_3 - a_2}{a_1} = (W_2 - W_1) \frac{w_{tr}}{a_1}, \quad (6)$$

Furthermore, the normalized transverse phase parameter  $U_1$  and the normalized transverse attenuation parameter  $W_1$  are defined as  $U_1^2 = a_1^2(k^2 n_{co}^2 - \beta^2)$  and  $W_1^2 = a_1^2(\beta^2 - k^2 n_{cl}^2)$ , respectively. Here,  $\beta$  is the propagation constant  $\beta = k_0 n_{eff}$ , where  $n_{eff}$  is the effective refractive index.  $V_1$  is the normalized frequency (which determines the number of modes) and satisfies the relationship  $V_1^2 = U_1^2 + W_1^2$ , defined as  $V_1 = ka_1 n_{co} (2\Delta_1)^{1/2}$ .

For parameters related to the trench structure (subscript 2), we define  $V_2 = ka_1(n_{cl}^2 - n_{tr}^2)^{1/2}$  and  $W_2^2 = V_2^2 + W_1^2$ . In these equations,  $k = 2\pi/\lambda$ , where  $\lambda$  is the vacuum wavelength.  $J_1$  and  $K_1$  represent the Bessel function of the first kind and the modified Bessel function of the second kind, respectively.

Utilizing the asymptotic expansion for large arguments, the expression in Eq(7). containing the modified Bessel function  $I_0$  can be approximated as:

$$I_0\left[\left(\frac{W_1}{a_1} + \frac{P_1 - P_2 + Y_1 - Y_2}{\Lambda - r}\right) r\right] \approx \sqrt{\tau} I_0\left(\frac{W_1}{a_1} r\right) \exp\left(\frac{P_1 - P_2 + Y_1 - Y_2}{\Lambda - r} r\right), \quad (7)$$

$\tau$  can be simplified to:

$$\tau = \frac{W_1/a_1}{W_1/a_1 + (P_1 - P_2 + Y_1 - Y_2)/\Lambda} = \frac{W_1}{W_1 + (W_2 - W_1)w_{tr}/\Lambda}, \quad (8)$$

Here,  $I_0$  is a function of  $r$ . The variable  $r$  is neglected because  $(P_1 - P_2 + Y_1 - Y_2)/(\Lambda - r)$  is much smaller than  $W_1/a_1$ , and  $r$  is much smaller than  $\Lambda$ . Substituting into Eq(5), the mode coupling coefficient between two adjacent cores of the trench-assisted MCF can be expressed as:

$$k_{pq} = \frac{\sqrt{\tau} \sqrt{\Delta_1}}{a_1} \frac{U_1^2}{V_1^3 K_1^2(W_1)} \sqrt{\frac{\pi a_1}{W_1 \Lambda}} \exp\left[-\frac{W_1 \Lambda + 2(W_2 - W_1)w_{tr}}{a_1}\right], \quad (9)$$

The average crosstalk (XT) between two adjacent cores in a homogeneous MCF can be expressed as<sup>[30]</sup>:

$$XT \approx \frac{2k_{pq}^2 R_b}{\beta \Lambda} L, \quad (10)$$

Where  $R_b$  is the bending radius, and  $L$  is the fiber length.

The coupling coefficient schematic for the seven-core fiber is shown in Fig. 1. When the light beam is incident on the fiber, the mode field distribution can be viewed as a superposition of individual modes within the  $7 \times 7$  weak coupling matrix<sup>[31-34]</sup>. If we designate the outer cores as Core 1 to Core 6 and the central core as Core 7, we obtain:

$$C = \begin{bmatrix} s_{11} & k_1 & 0 & 0 & 0 & k_1 & k_1 \\ k_1 & s_{22} & k_1 & 0 & 0 & 0 & k_1 \\ 0 & k_1 & s_{33} & k_1 & 0 & 0 & k_1 \\ 0 & 0 & k_1 & s_{44} & k_1 & 0 & k_1 \\ 0 & 0 & 0 & k_1 & s_{55} & k_1 & k_1 \\ 0 & 0 & 0 & 0 & k_1 & s_{66} & k_1 \\ k_1 & k_1 & k_1 & k_1 & k_1 & k_1 & s_{77} \end{bmatrix}, \quad (11)$$

Here,  $s_{pp}$  represents the self-coupling coefficient, while  $k_{pq}$  represents the inter-core coupling coefficient. Due to the weakly coupled characteristics of this fiber design, coupling between non-adjacent cores can be ignored; therefore,  $k_2$  and  $k_3$  are approximated as zero.

When  $\Lambda = 10 \mu\text{m}$ , the intrinsic mode distribution of the fiber at a center wavelength of 1550 nm

is illustrated in Fig. 4. In stark contrast to the weakly coupled design objective, this figure clearly exhibits the characteristics of the seven-core fiber in a strongly coupled state. Due to the small core pitch and the weak optical confinement provided by the trenches, the independent mode fields of the cores overlap and degenerate, forming super-modes distributed across the entire fiber cross-section<sup>[34]</sup>. Consequently, the optical field energy is no longer confined within individual cores but demonstrates a significant delocalization distribution among the seven cores. This strong coupling phenomenon results in excessively high inter-core crosstalk, making it impossible to support signal transmission in independent channels.

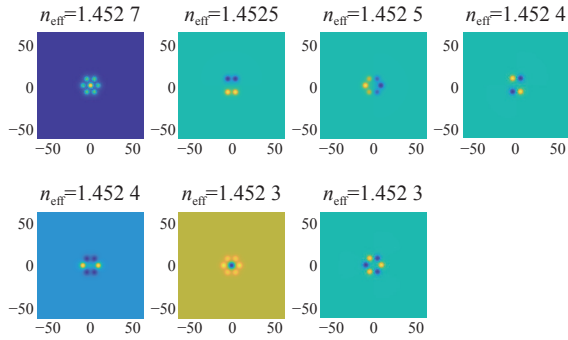


Fig. 4 super-modes and refractive index profile

In contrast, when the parameter combinations listed in Tab. 1 are adopted, the fiber mode distribution reverts to a weakly coupled state. It is worth noting that the emergence of strongly coupled super-modes in Fig. 4 visually reveals the sensitivity of the fiber structural parameter design: improper parameter selection (such as an excessively small core pitch or insufficient refractive index difference) causes the fiber to degenerate into a strongly coupled device. This further substantiates the necessity of introducing the Particle Swarm Optimization (PSO) algorithm for global optimization; specifically, it is essential to precisely search for the optimal parameter space capable of breaking strong coupling and achieving ultra-low crosstalk under standard cladding dimension constraints.

From a physical perspective, the transition

from the strongly coupled super-modes shown in Fig. 4 to a weakly coupled state is achieved by the optimized trench design. The introduction of the low-refractive-index trench (with optimized width  $w_{tr}$  and depth  $\Delta_2$ ) creates a deep potential barrier for the optical field. This barrier effectively suppresses the evanescent wave tail of the fundamental mode, significantly reducing the mode field overlap integral ( $k_{pq}$ ) between adjacent cores. Consequently, the coupling coefficient drops below the threshold required for super-mode formation, forcing the optical energy to be tightly confined within individual cores and ensuring independent signal transmission.

Exploring all parameter combinations in Tab. 1 involves a vast number of permutations. The central core is subject to the greatest coupling influence from the surrounding cores, involving six coupling coefficients between it and the adjacent cores. Each outer core is associated with three coupling coefficients with its adjacent cores. However, since the pitch between non-adjacent cores is relatively large ( $>30 \mu\text{m}$ ), their mutual coupling is negligible. The final inter-core crosstalk is expressed as:

$$\overline{XT} = \frac{XT_1 + XT_2 + \dots + XT_{12}}{12}, \quad (12)$$

### 3.2 Combination of Constraints

The MCF design in this paper incorporates the following six constraints. Beyond coating loss, five specific tests were conducted for all MCF designs:

(a) Geometric Overlap: To prevent structural overlap between adjacent cores, the spacing between the edges of the trenches must remain positive. Based on the core pitch  $\Lambda$  and the outer trench radii of adjacent cores ( $a_{r,i} + a_{r,j}$ ),

this constraint is expressed as:

$$\text{EdgeS pacing} = \Lambda - (a_{r,i} + a_{r,j}) > 0 \mu\text{m}, \quad (13)$$

If this constraint is violated, a penalty of  $10^7$  is directly applied to the fitness value, and subsequent calculations are skipped, significantly lowering the

priority of this design.

(b) Induced Loss: The induced loss caused by the central core must be less than 0.001 dB/km<sup>[35]</sup>. The crosstalk between adjacent cores can be expressed as<sup>[36]</sup>:

$$\overline{XT} \approx \eta L \approx \frac{2k_{pq}^2 R_b}{\beta \Lambda} L \quad (14)$$

where  $\eta$  is the power coupling coefficient,  $k_{pq}$  is the mode coupling coefficient,  $R_b$  is the bending radius,  $\beta$  is the propagation constant, and  $L$  is the fiber length. In this seven-core fiber, due to crosstalk (XT) to other cores, the optical power launched into and propagating through the central core decays along the propagation direction at a rate of  $6\eta$ . When the XT is sufficiently low, the power attenuation can be approximated as  $\exp(-6\eta L)$ , and the crosstalk-induced loss of the central core ( $\alpha_{XT}$ [dB]) can be estimated as:

$$\alpha_{XT} \approx -10 \log_{10} [\exp(-6\eta L)] = (10 \ln 10) 6\eta L, \quad (15)$$

The relationship is shown in Fig. 5. As illustrated, the crosstalk-induced loss increases linearly with the power coupling coefficient. This direct correlation allows us to determine the upper limit of the coupling coefficient required to maintain the additional loss below the target threshold of 0.001 dB/km. To suppress this value below 0.001 dB/km, the value of  $\eta$  should be less than  $9.4 \times 10^{-4}$  (corresponding to  $L=100$  km). Similarly, if this constraint is violated, a penalty of  $10^7$  is directly applied to the fitness value.

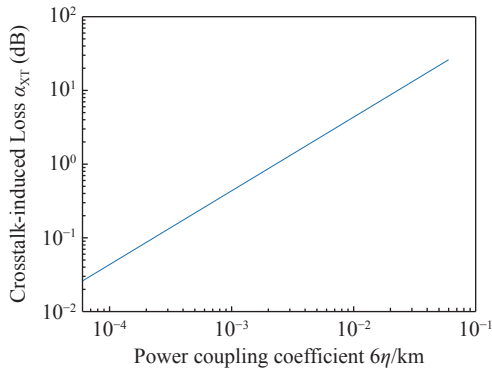


Fig. 5 Crosstalk-induced Loss vs. Power Coupling Coefficient at 100 km

(c) Full-band Dispersion Constraint: To ensure consistent transmission performance across the C-band and L-band, the total dispersion value of the fiber throughout the operating wavelength range (1530 nm~1625 nm) should satisfy  $16.87 \leq D(\lambda) \leq 27.13$  ps/(nm·km). If the dispersion exceeds this range, the penalty value is the square of the difference between the actual dispersion value and the boundary mean (22 ps/(nm·km)).

$$PenaltyD = \begin{cases} (D - 22)^2 & \text{if } D < 14.87 \text{ or } D > 27.13 \\ 0 & \text{otherwise} \end{cases}, \quad (16)$$

Excessive dispersion leads to signal distortion, while dispersion that is too low may limit bandwidth utilization. Fig. 6 and Fig. 7 display the dispersion parameter ( $\beta_0, \beta_1, \beta_2, \beta_3$ ) curves varying with wavelength for the minimum and maximum parameter combinations in Tab.1, respectively. The physical quantities corresponding to these dispersion parameters are the propagation constant, group delay, Group Velocity Dispersion (GVD), and dispersion slope, respectively.

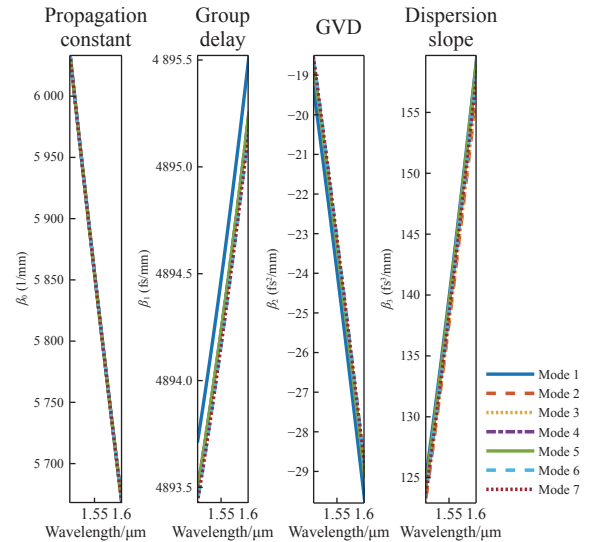


Fig. 6 Dispersion characteristics of minimum parameter combination optical fiber mode

It can be seen that in each order of dispersion, all modes of the fiber exhibit the same trend. The values of  $\beta_0$  and  $\beta_2$  decrease with increasing center

wavelength, while the values of  $\beta_1$  and  $\beta_3$  are positively correlated with the center wavelength. Within the C-band and L-band, all modes satisfy  $\beta_2 < 0$ , indicating that this homogeneous doped MCF transmits in the anomalous dispersion regime. Next, we will use  $\beta_2$  to determine the fiber's dispersion. The expression for dispersion is:

$$D = -\frac{2\pi c}{\lambda^2} \beta_2, \quad (17)$$

Based on the above formula, we calculated the dispersion distribution for the parameter combinations before and after optimization. display the dispersion values in the C+L band for the minimum and maximum parameter combinations listed in Tab. 1, respectively. As seen in the figures, with the minimum parameter combination (Fig. 8), the dispersion values range between [16.87, 23.25] ps/(nm·km) across the 1530 nm to 1625 nm range; with the maximum parameter combination (Fig. 9), the dispersion values fall within the [21.60, 27.13] ps/(nm·km) interval. This demonstrates that even under boundary conditions where structural parameters vary to their limits, the optimized fiber dispersion strictly remains within the preset constraint range of  $16.87 \leq D(\lambda) \leq 27.1$  ps/(nm·km), ensuring compatibility with standard single-mode fiber transmission characteristics.

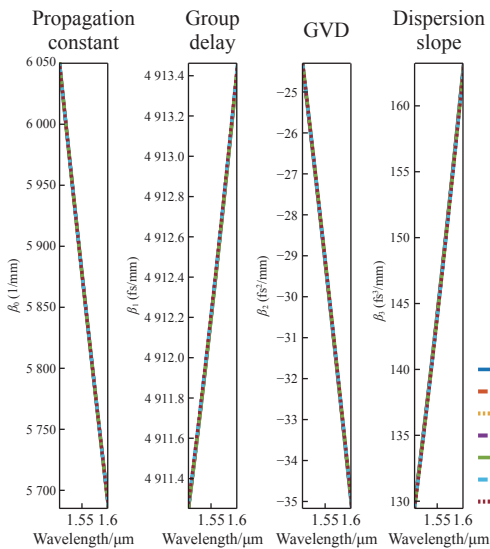


Fig. 7 Dispersion characteristics of maximum parameter combination optical fiber mode

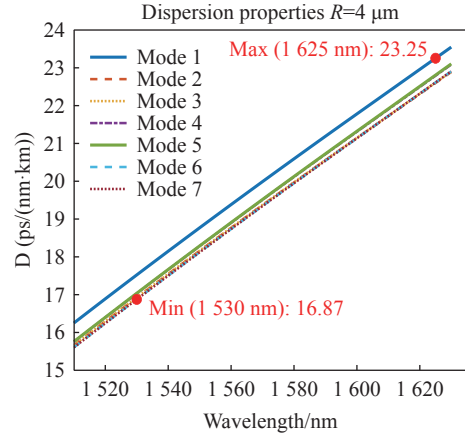


Fig. 8 Minimum parameter combination fiber dispersion value

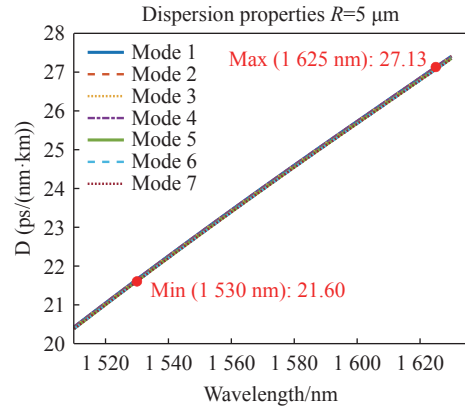


Fig. 9 Maximum parameter combination fiber dispersion value

(d) Effective Normalized Frequency  $V_{eff} < 2.405$ : To ensure high-quality signal transmission, the fiber must strictly maintain Single-Mode Operation (SMO) to eliminate inter-modal dispersion. For standard step-index fibers, the condition for SMO is defined as a normalized frequency  $V < 2.405$ . However, in the design of the trench-assisted MCF used in this study, the presence of low-refractive-index trenches significantly alters the mode cutoff characteristics, making the traditional  $V$ -value definition no longer accurate. To accurately predict the single-mode cutoff condition for this complex refractive index profile, this paper introduces the effective normalized frequency  $V_{eff}$ . This parameter is based on the Equivalent Step-Index (ESI) model concept, which equates the complex trench structure to a step-index fiber with identical cutoff characteristics, thereby allowing the classical single-

mode criterion to remain applicable. This modified parameter is combined with the effective relative refractive index difference  $\Delta_{eff}$  for correction, defined as follows:

$$V_{eff} = \frac{2\pi a}{\lambda_c} n_{co} \sqrt{2\Delta_{eff}} \quad , \quad (18)$$

$$\Delta_{eff} = \frac{n_{co}^2 - n_{eff}^2}{2n_{co}^2} \quad , \quad (19)$$

Where  $\lambda_c$  is the cutoff wavelength, and  $n_{eff}$  represents the equivalent refractive index of the actual light field propagation after considering the trench structure. This parameter can be obtained via Finite Element Method (FEM) simulation or estimated using analytical expressions. According to reference<sup>[28]</sup>, the trench structure results in  $\Delta_{eff} < \Delta_1$ , thereby significantly reducing  $V_{eff}$ , which is conducive to maintaining single-mode transmission. Similarly, if this constraint is violated, a penalty of magnitude  $10^7$  is directly applied to the fitness value.

(e) Effective Mode Field Area ( $A_{eff}$ ): A smaller  $A_{eff}$  enhances nonlinear effects, while an excessively large  $A_{eff}$  may lead to mode instability. The formula for calculating the effective mode field area is as follows:

$$A_{eff} = \frac{\left( \iint |E|^2 dx dy \right)^2}{\iint |E|^4 dx dy} \quad , \quad (20)$$

Selecting the minimum and maximum parameter combinations from Tab. 1, the calculated effective mode field areas are  $84.6 \mu\text{m}^2$  and  $175.2 \mu\text{m}^2$ , respectively. It can also be expressed using the mode field radius ( $W_L$ ):

$$A_{eff} = \pi W_L^2 \quad , \quad (21)$$

For step-index fibers, the expression for the mode field radius can be represented as<sup>[37]</sup>:

$$\frac{W_L}{a_1} \approx 0.65 + \frac{1.619}{V^{3/2}} + \frac{2.879}{V^6} \quad , \quad (22)$$

Where  $a_1$  is the core radius and  $V$  represents the normalized frequency. Combining this expression

with Eq(18) (i.e., replacing  $V$  with  $V_{eff}$ ), we can derive the joint constraint relationship between the fiber's effective mode field area and the cutoff wavelength.

Through the above analysis, it can be seen that PSO explores the maximum effective mode field area ( $A_{eff}$ ) constraint satisfiable under each cutoff wavelength constraint through the combination of various constraints, as shown in Fig. 10. It starts from the widest bandwidth (cutoff wavelength  $\leq 1360$  nm) and the minimum  $A_{eff}$  constraint ( $A_{eff} \in [85, 115] \mu\text{m}^2$ ). For each constraint combination, the Particle Swarm Optimization algorithm is run 100 times to test its reliability.

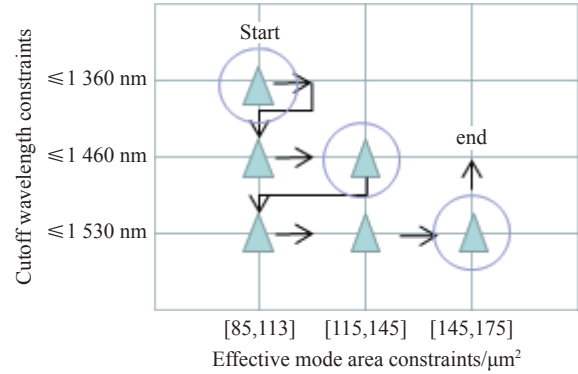


Fig. 10 Constraint combination

Next, we focus only on the MCF parameter solutions obtained under the highest  $A_{eff}$  constraint and the corresponding cutoff wavelength range, which corresponds to the solution within the purple circle in Fig. 11. At the beginning of the objective function calculation, constraints such as coating loss, geometric non-overlap, and induced loss caused by the central core are checked first. If these three constraints are all satisfied, the fitness function is:

$$\begin{aligned} \text{Fitness} = & XT + \text{Penalty } A_{eff} + \\ & \text{Penalty Dispersion} + \\ & \text{Penalty cutoff - wavelength} \quad , \quad (23) \end{aligned}$$

If any of these conditions are not met, the fitness value will be assigned a huge penalty value of magnitude  $10^7$ . In this way, we further reduce the problem space and shorten the computation time.

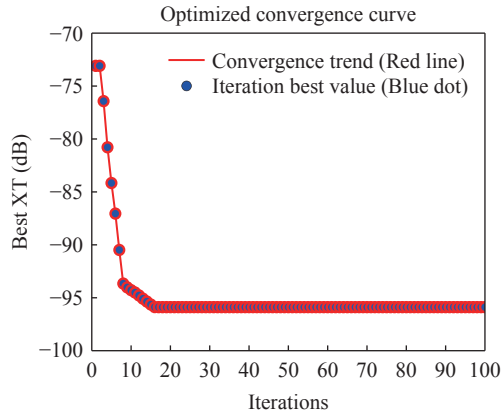


Fig. 11 Optimized convergence curve (Each red circle represents an iteration)

### 3.3 Optimization Parameters and Performance Analysis

For each constraint combination emphasized in Fig. 10, the PSO algorithm was executed 100 times, and solutions satisfying all constraints were obtained in all cases. The bending radius was set to 210 mm at a wavelength of 1550 nm. In these four scenarios, based on the calculation and assessment of the constraint combinations, solutions satisfying the constraints exist for Case 1 ( $\lambda \leq 1360$  nm). However, for Case 2 ( $\lambda \leq 1460$  nm) and Case 3 ( $\lambda \leq 1530$  nm), the range of  $A_{eff}$  must be narrowed to satisfy the conditions. The minimum crosstalk obtained in Case 1 is -95.89 dB/km. Through data analysis and simulation, the following results can be derived:

Fig. 11 illustrates the variation of the fitness function values during the iteration process. As the number of iterations increases, the design parameters gradually converge to the optimal solution. When the iteration count reaches 100, the optimal values for  $a_1, w_{cl}, w_{tr}, \Delta_1, \Delta_2$  and  $\Lambda$  in Tab.1 correspond to 4.3  $\mu\text{m}$ , 4.9  $\mu\text{m}$ , 7.5  $\mu\text{m}$ , 0.0045, -0.007, and 45  $\mu\text{m}$ , respectively.

Fig. 12 and Fig. 13 illustrate the relationship between crosstalk and core radius/core pitch when  $\Delta_1$  is 0.6% and  $\Delta_2$  is -0.7%; and the relationship between crosstalk and the refractive index differences of the trench and core when  $a_1$  is 4.25  $\mu\text{m}$  and the core pitch is 40  $\mu\text{m}$ . With other parameters held

constant, the results confirm that increasing the core pitch and introducing the trench structure play a critical role in crosstalk suppression, particularly given the exponential sensitivity of crosstalk to these variations. Fig. 14 displays the trend of inter-core crosstalk (XT) in the optimized seven-core fiber as the transmission distance  $L$  increases. Simulation results indicate that when the transmission distance increases from 1 km to 200 km, the XT value rises from an initial -100 dB/km to -75 dB/km.

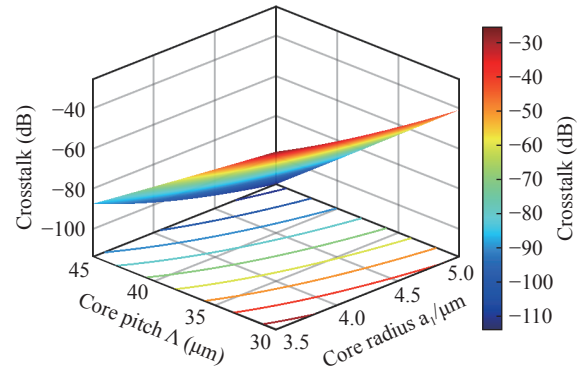


Fig. 12 TA-MCF Crosstalk vs Core Radius and Pitch

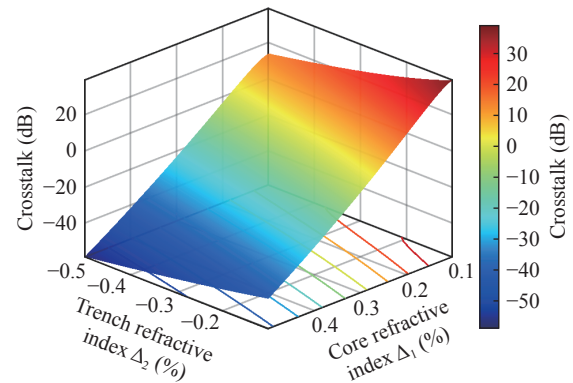


Fig. 13 TA-MCF Crosstalk vs  $\Delta_1$  and  $\Delta_2$

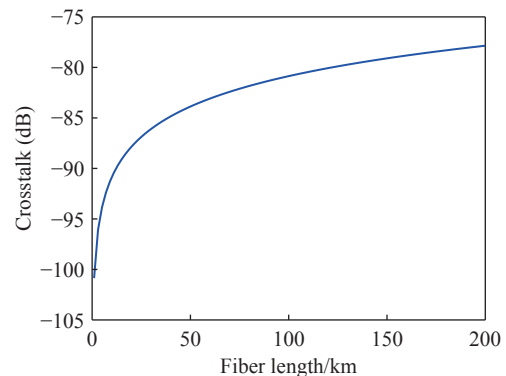


Fig. 14 TA-MCF Crosstalk vs Fiber Length

This trend is consistent with the theoretical prediction in Eq(10), validating the linear characteristic of crosstalk accumulation with distance under the weak coupling mechanism.

### 3.4 Fabrication Tolerance and Bending Analysis

In practical deployment, fibers may experience tighter bends than the standard 210 mm radius. According to Eq. (10), inter-core crosstalk is linearly proportional to the bending radius. Therefore, under a tighter bending radius (e.g.,  $R_b=30$  mm), the crosstalk will be theoretically lower than the value at 21 mm due to the increased phase mismatch between cores. Specifically, at  $R_b=30$  mm, the crosstalk is suppressed by approximately 8.4 dB compared to 210 mm. Although tighter bends typically induce higher macro-bending loss, the optimized trench structure in this design provides strong mode confinement, keeping the macro-bending loss negligible ( $<0.1$  dB/turn) even at a 30 mm radius.

Furthermore, considering the fabrication limits, we analyzed the impact of structural deviations. Fig. 15 illustrates the variation of crosstalk and dispersion when the core radius ( $a_1$ ) deviates by  $\pm 1\%$ . As shown in the figure, the inter-core crosstalk exhibits a variation of approximately 5 dB but consistently remains below  $-87$  dB/km (ranging from  $-92$  dB/km to  $-87$  dB/km). Meanwhile, the dispersion variation is controlled within  $1.3$  ps/(nm·km) (ranging from  $21.4$  to  $22.7$  ps/(nm·km)), which satisfies the design requirements for the C+L band.

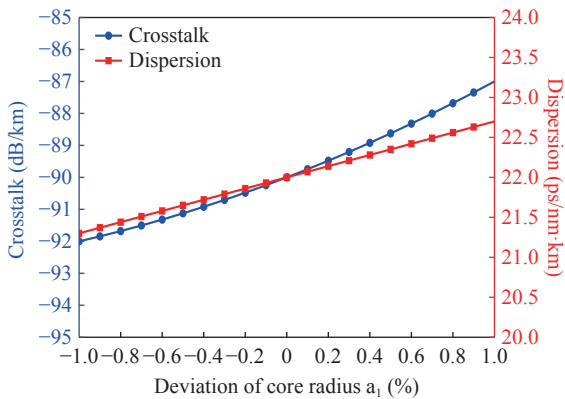


Fig. 15 Variations of crosstalk and dispersion under  $\pm 1\%$  deviation of core radius

This demonstrates that the proposed fiber design exhibits high robustness against typical manufacturing errors.

## 4 Conclusion

In this paper, the Particle Swarm Optimization (PSO) algorithm was employed to optimize all parameters of a weakly coupled trench-assisted seven-core fiber. Unlike previous methods limited to local parameter scanning or relying on complex heterogeneous structures, this global optimization strategy effectively balanced conflicting physical constraints. Consequently, coordinated control of crosstalk, effective mode field area, and dispersion was achieved. Specifically, while maintaining the standard  $125$   $\mu\text{m}$  cladding diameter, the optimized fiber achieved a large effective mode field area consistent with standard single-mode fibers, as well as a dispersion range of  $16.87$  to  $27.13$  ps/(nm·km).

Based on the finally optimized structural parameters, the calculated mode coupling coefficient is approximately  $3.735 \times 10^{-3} \text{m}^{-1}$ , corresponding to a theoretical coupling length of approximately  $420.5$  m. This value far exceeds the typical transmission span, strictly validating the realization of the weakly coupled regime from a physical mechanism. The results demonstrate that the optimized fiber achieves an ultra-low crosstalk of  $-90$  dB/km at  $1550$  nm, significantly enhancing optical communication capacity and providing strong technical support for future high-speed, large-capacity optical communication networks. To visually demonstrate the performance advantages of this design, Tab. 2 compares the proposed fiber with other representative 7-core fiber designs.

As shown in Tab.2, our optimized design achieves a superior balance, offering significantly lower crosstalk and a larger effective mode area compared to existing designs under similar dimensional constraints.

Data analysis during the iteration process indic-

ates that as parameters converge to the optimal solution, the effectiveness of the core and the surrounding low-refractive-index trench within the fiber cross-section is verified. Numerical simulations further prove that precise adjustment of the trench can yield significant performance improvements. Key

parameters such as trench width, inner cladding width, and the refractive index differences between layers can effectively control the degree of inter-core crosstalk, which is helpful to improve the capacity and reliability of the whole optical communication system.

**Tab. 2 Comparison with other 7-core fiber designs**

Reference	Structure Type	Core Pitch ( $\mu\text{m}$ )	Crosstalk (dB/km)	$A_{eff}(\mu\text{m}^2)$
Ref. [11]	Trench-assisted	45	~50	80
Ref. [13]	Channel-assisted	35~45	-66(@1310 nm)	-
This work	Optimized Trench	45	<-90	~110

## References:

- [1] HOSSEINI S, DE MIGUEL I, MERAYO N, *et al.*. Energy efficient multipath routing in space division multiplexed elastic optical networks[J]. *Computer Networks*, 2024, 244: 110349.
- [2] TIWARI K, BATHAM D, THAKARE V. Space division multiplexing elastic optical network—challenges and opportunities[C]. *Proceedings of ICSISCET 2022 on Artificial Intelligence and Sustainable Computing*, Springer, 2022: 345-357.
- [3] CHEN W P, YUAN L, ZHANG B, *et al.*. Applications and development of multi-core optical fibers[J]. *Photonics*, 2024, 11(3): 270.
- [4] HAYASHI T, SAKAMOTO T, YAMADA Y, *et al.*. Randomly-coupled multi-core fiber technology[J]. *Proceedings of the IEEE*, 2022, 110(11): 1786-1803.
- [5] HAYASHI T, NAGASHIMA T, INOUE A, *et al.*. Uncoupled multi-core fiber design for practical bidirectional optical communications[C]. *2022 Optical Fiber Communications Conference and Exhibition (OFC)*, IEEE, 2022: 1-3.
- [6] 李增辉, 李曙光, 李建设, 等. 一种具有低串扰低非线性的双沟槽环绕型十三芯五模光纤[J]. *物理学报*, 2021, 70(10): 104208.
- [7] LI Z H, LI SH G, LI J SH, *et al.*. Double-trench assisted thirteen-core five-mode fibers with low crosstalk and low non-linearity[J]. *Acta Physica Sinica*, 2021, 70(10): 104208. (in Chinese).
- [8] WINZER P J, NEILSON D T, CHRAPLYVY A R. Fiber-optic transmission and networking: the previous 20 and the next 20 years [Invited] [J]. *Optics Express*, 2018, 26(18): 24190-24239.
- [9] XIA C, AMEZCUA-CORREA R, BAI N, *et al.*. Hole-assisted few-mode multicore fiber for high-density space-division multiplexing[J]. *IEEE Photonics Technology Letters*, 2012, 24(21): 1914-1917.
- [10] ZHU J H, LAN D, LIU X H, *et al.*. Porous structure fibers based on multi-element heterogeneous components for optimized electromagnetic wave absorption and self-anticorrosion performance[J]. *Small*, 2024, 20(47): 2403689.
- [11] PUTTNAM B J, RADEMACHER G, LUÍS R S. Space-division multiplexing for optical fiber communications[J]. *Optica*, 2021, 8(9): 1186-1203.
- [12] TAKENAGA K, ARAKAWA Y, TANIGAWA S, *et al.*. Reduction of crosstalk by trench-assisted multi-core fiber[C]. *2011 Optical Fiber Communication Conference and Exposition and the National Fiber Optic Engineers Conference*, IEEE, 2011: 1-3.
- [13] TU J J, SAITOH K, KOSHIBA M, *et al.*. Design and analysis of large-effective-area heterogeneous trench-assisted multi-core fiber[J]. *Optics Express*, 2012, 20(14): 15157-15170.
- [14] HAYASHI T, NAGASHIMA T, MORISHIMA T, *et al.*. Multi-core fibers for data center applications[C]. *45 th European Conference on Optical Communication (ECOC 2019)*, IET, 2019: 1-4.
- [15] YE F H, TU J J, SAITOH K, *et al.*. Design of homogeneous trench-assisted multi-core fibers based on analytical

- model[J]. *Journal of Lightwave Technology*, 2016, 34(18): 4406-4416.
- [15] ZHANG L, LI J, WANG Y, *et al.*. Ultra-low crosstalk trench-assisted heterogeneous 7-core fiber for wideband transmission[J]. *Optical Fiber Technology*, 2024, 82: 103612. (查阅网上资料, 未找到本条文献信息, 请确认).
- [16] PUTTNAM B J, LUÍS R S, RADEMACHER G, *et al.*. 319 Tb/s transmission over 3001 km with S, C and L band signals over >120 nm bandwidth in 125  $\mu\text{m}$  wide 4-core fiber[C]. *2021 Optical Fiber Communications Conference and Exhibition (OFC)*, IEEE, 2021: 1-3.
- [17] SASAKI T, TAKENAGA K, MATSUO S. Inter-core crosstalk reduction in trench-assisted multicore fibers with optimized structural parameters[J]. *Journal of Lightwave Technology*, 2023, 41(4): 1205-1212. (查阅网上资料, 未找到本条文献信息, 请确认).
- [18] WANG Y ZH, FUJISAWA T, SAKAMOTO T, *et al.*. Step index 8-core fiber with 125- $\mu\text{m}$  cladding diameter for O-band use[C]. *2020 Opto-Electronics and Communications Conference (OECC)*, IEEE, 2020: 1-3.
- [19] JIANG SH L, MA L, VELAZQUEZ M N, *et al.*. Design of 125- $\mu\text{m}$  cladding diameter multicore fibers with high core multiplexing factor for wideband optical transmission[J]. *Optical Fiber Technology*, 2019, 50: 55-61.
- [20] WANG Y ZH, FUJISAWA T, SAGAE Y, *et al.*. A novel core allocation in heterogeneous step-index multi-core fibers with standard cladding diameter[J]. *Journal of Lightwave Technology*, 2021, 39(22): 7231-7237.
- [21] WANG C, YANG F, LI Z. Global optimization of multicore fiber parameters based on improved particle swarm optimization algorithm[J]. *Acta Optica Sinica*, 2023, 43(15): 1506002. (查阅网上资料, 未找到本条文献信息, 请确认).
- [22] MATA J, DE MIGUEL I, DURÁN R J, *et al.*. Supervised machine learning techniques for quality of transmission assessment in optical networks[C]. *2018 20 th International Conference on Transparent Optical Networks (ICTON)*, IEEE, 2018: 1-4.
- [23] SAKAMOTO T, MORI T, WADA M, *et al.*. Strongly-coupled multi-core fiber and its optical characteristics for MIMO transmission systems[J]. *Optical Fiber Technology*, 2017, 35: 8-18.
- [24] BHOWMIK K, PENG G D. Polymer optical fibers[M]//PENG G D. Handbook of Optical Fibers. Singapore: Springer, 2019: 967-1017.
- [25] LIU H, HUANG B, REN G. Design of large effective area trench-assisted multicore fiber with low differential mode delay[J]. *Optics Communications*, 2022, 508: 127768. (查阅网上资料, 未找到本条文献信息, 请确认).
- [26] HAYASHI T, TARU T, SHIMAKAWA O, *et al.*. Characterization of crosstalk in ultra-low-crosstalk multi-core fiber[J]. *Journal of Lightwave Technology*, 2012, 30(4): 583-589.
- [27] WANG F, QIU Y H. A modified particle swarm optimizer with roulette selection operator[C]. *2005 International Conference on Natural Language Processing and Knowledge Engineering*, IEEE, 2005: 765-768.
- [28] CLERC M, KENNEDY J. The particle swarm - explosion, stability, and convergence in a multidimensional complex space[J]. *IEEE Transactions on Evolutionary Computation*, 2002, 6(1): 58-73.
- [29] YE F H, TU J J, SAITOH K, *et al.*. Simple analytical expression for crosstalk estimation in homogeneous trench-assisted multi-core fibers[J]. *Optics Express*, 2014, 22(19): 23007-23018.
- [30] XIA C, EFTEKHAR M A, CORREA R A, *et al.*. Supermodes in coupled multi-core waveguide structures[J]. *IEEE Journal of Selected Topics in Quantum Electronics*, 2016, 22(2): 196-207.
- [31] JIN W X, JIAN SH SH. Numerical and simulation analyses on supermode characteristics of dual-core fiber and four-core fiber[J]. *Optik*, 2017, 132: 32-38.
- [32] CHEN Y, ZHAO X, LIU S. Bending-insensitive weakly coupled multicore fiber with air-hole-assisted trench structure[J]. *IEEE Photonics Journal*, 2025, 17(1): 7100408. (查阅网上资料, 未找到本条文献信息, 请确认).
- [33] ZHENG S W, REN G B, LIN ZH, *et al.*. Mode-coupling analysis and trench design for large-mode-area low-cross-talk multicore fiber[J]. *Applied Optics*, 2013, 52(19): 4541-4548.
- [34] 方晓慧. 多芯光子晶体光纤飞秒激光系统及其在频率变换中的应用[D]. 天津: 天津大学, 2010.  
FENG X H. *Multi-core photonic crystal fiber femtosecond laser system and its applications in frequency conversion*[D]. Tianjin: Tianjin University, 2010. (in Chinese).
- [35] KASAHARA M, SAITOH K. Design and analysis of 4-LP mode 12-core fiber for high-density space-division multiplexing[J]. *Journal of Lightwave Technology*, 2022, 40(11): 3482-3489. (查阅网上资料, 未找到本条文献信息, 请确认).

- [36] HAYASHI T, TARU T, SHIMAKAWA O, *et al.*. Design and fabrication of ultra-low crosstalk and low-loss multi-core fiber[J]. *Optics Express*, 2011, 19(17): 16576-16592.
- [37] PAN O, JIA Y D, BAI M, *et al.*. *Advanced Optical Simulation (MATLAB Version): Optical waveguides, Lasers*[M]. 2014. (查阅网上资料, 未找到本条文献信息, 请确认).

Author Biography:



ZHAN Yi (1969—), female, from Rizhao, Shandong Province. Ph.D., Professor, and Doctoral Supervisor. She received her Ph.D. degree in Materials Science and Engineering from Zhengzhou University in 2007. Her research focuses on optical fiber nonlinearities and ultrafast laser generation mechanisms of nanomaterials. Current interests include the mode-locking mechanism and device design of fiber lasers based on chalcogenide nanocrystals. E-mail: [zhanyi@qfnu.edu.cn](mailto:zhanyi@qfnu.edu.cn)